scientific reports

OPEN

Nucleation and stability of skyrmions in three-dimensional chiral nanostructures

Yan Liu✉, Na Cai, Xingxing Yu & Shengjie Xuan

We studied the magnetization evolution in three-dimensional chiral nanostructures, including nanotubes and circularly curved thin films, by micromagnetic simulations. We found that in a nanotube skyrmions can be formed by broken of the helical stripes on the left and right sides of the nanotube, and the formation of skyrmions doesn't correspond to any abrupt change of topological number. Skyrmions can exist in a large range of magnetic field, and the thinner nanotube has a larger field range for skyrmion existence. The configuration of a skyrmion in nanotubes is different from the one in thin film. From the outer to the inner circular layer, the size of the skyrmion becomes larger, and the deformation becomes more obvious. In circularly curved magnetic films with fixed arc length, there are three kinds of hysteresis processes are found. For the curved films with a large radius, the magnetization evolution behavior is similar to the case in two-dimensional thin films. For the curved films with a small radius, the skyrmions are created by broken of the helical stripes on the left and right sides of the curved film. For the curved film with a medium radius, no skyrmion is formed in the hysteresis process.

The topic of magnetism in curved geometry has attracted much attention in modern magnetism research. Curvature effect has been emerged as an efficient means to impact the statics and dynamics of magnetic texture[1–3]. It may bring the emergence of unconventional spin textures, where novel physical effects comprising geometry, topology, and chirality[3–7]. It has demonstrated that curvature will induce two additional energies: geometrically induced-anisotropy energy and effective Dzyaloshinskii-Moriya interaction (DMI) energy[3,4,8]. These additional energies excite many striking novel properties in three-dimensional curved magnetic thin films, wires, and nanotubes, such as magnetochiral effects[9,10], topologically induced magnetic patterns[11], and Spin-Cherenkov effect of spin waves[12].

Magnetic skyrmions are stable spin textures with the magnetic moments forming a twist structure. The key characteristic is they are topological protected. They have been widely considered as data carriers in spintronics[13–18]. It is known that skyrmions are rather peculiar topological magnetic structures and they have been observed in several classes of magnetic materials without inversion symmetry[13–26]. Both DMI energy and anisotropy energy have an obvious effect on the stability of skyrmions[14,27]. Therefore, the interplay between skyrmions and curvature is worthy to investigate. It was reported that skyrmions may be stabilized by curvature effects only in a spherical shell[28,29], and skyrmions can be the ground state when its radius is comparable with the size of curvilinear defect of a thin magnetic film[30]. More recently, Wang et al. reported that skyrmions can move in magnetic nanotubes in presence of very large current density without annihilation[31], and we also demonstrated that skyrmions can exist in a nanotube[32].

In this work, we introduce curvature into chiral magnetic materials to investigate the magnetization evolution in three-dimensional chiral nanostructures, including nanotubes and curved thin films. We use micromagnetic simulation to describe how the characteristic properties such as the skyrmion nucleation and annihilation and its structure depending on the size of nanostructures. Indeed, those three-dimensional magnetic structures with complicated geometries and different sizes have been fabricated by various chemical and physical approaches[7,33–35], which may make our simulations be experimentally measured.

Method

The magnetization dynamics in chiral nanostructures is described by the Landau–Lifshitz–Gilbert (LLG) equation:

College of Sciences, Northeastern University, Shenyang 110819, People's Republic of China. ✉email: liuyanphys@mail.neu.edu.cn

Figure 1. (**a**) The sketch of the nanotube. Its length is fixed at $L = 400$ nm, its outer and inner radius are denoted ▶ by R and r, respectively. The Cartesian coordinates and the cylindrical coordinates used for the analytic study are sketched in the inset of this figure, where r_z is the radius of a circular layer, and s_{arc} is the arc length from the line $y = 0$ for a fixed r_z. (**b**) The topological number as a function of H_z in a nanotube when a z-direction magnetic field is applied, where $R = 40$ nm and $r = 20$ nm. Three regions are depicted in this figure, where I is the region of twisted helical stripe state, II is the region of skyrmions, and III is the region of ferromagnetic state. (**c**)–(**f**) The snapshot of the magnetic state at different H_z. The left panel is the three-dimensional magnetic configurations of the nanotube. The arrows represent the magnetic moment, and the color encodes the z component of the magnetization, The color scale is shown on the top. The right panel is m_z-image in x-s_{arc} plane for $r_z = 39$ nm.

$$\dot{\mathbf{m}} = -\gamma \mathbf{m} \times \mathbf{H}_{\text{eff}} + \alpha \mathbf{m} \times \dot{\mathbf{m}}, \tag{1}$$

where γ is the gyromagnetic ratio, α is the Gilbert damping constant, and $\mathbf{m}$ is the unit vector representing the orientation of the magnetization. The effective magnetic field is given by $\mathbf{H}_{\text{eff}} = -1/(\mu_0 M_s)(\partial W / \partial \mathbf{m})$, where W is the magnetic energy of the nanodisk consisting of exchange, DMI, magnetostatic, and Zeeman energy terms. The LLG equation is solved by using the Mumax code[36]. In the simulation, the nanotube is discretized into many small cells with a cell size of $2 \times 2 \times 2$ nm^3. The material parameters used for the simulations corresponding to FeGe[37]: saturation magnetization $M_s = 3.84 \times 10^5$ A/m, the exchange constant $A = 8.78 \times 10^{-12}$ J/m, DMI constant $D = 1.58 \times 10^{-3}$ J/m^2,and the Gilbert damping constant $\alpha = 0.2$.

In order to clarify different observed magnetization configurations in three-dimensional nanostructures, we calculated the topological number of the system. As is well known, in a two-dimensional plane the topological number is defined as

$$Q = \frac{1}{4\pi} \int \mathbf{m} \cdot \left(\frac{\partial \mathbf{m}}{\partial x} \times \frac{\partial \mathbf{m}}{\partial y} \right) dx dy. \tag{2}$$

The topological number is defined as a measure of the wrapping of $\mathbf{m}$ around a unit sphere, which allows to show the change of the magnetization configuration in the system, for example, the formation of skyrmions[38]. Also, it can be used to counting the number of skyrmions. In our model, the magnetic states reside in a curved film. To calculate the topological number in such geometry, we first choose the magnetization data in a circular layer with a fixed radius r_z (Fig. 1a), and then we calculate the topological number of the skyrmion in this circular layer as

$$Q = \frac{1}{4\pi} \int \mathbf{m} \cdot \left(\frac{\partial \mathbf{m}}{\partial x} \times \frac{\partial \mathbf{m}}{\partial s} \right) dx ds, \tag{3}$$

where $ds = \sqrt{(dy)^2 + (dz)^2}$ is the differential arc.

In this paper, the sample is a three-dimensional geometry. To show the magnetic states in this geometry more clearly, besides the three-dimensional images, we also show the m_z-image in a two-dimensional plane. We first choose the data in a circular film that satisfy the condition $r_z - 2$ nm $< \sqrt{y^2 + z^2} < r_z$. Then we take x as X-axis, s_{arc} as Y-axis, where s_{arc} is the arc length from the line $y = 0$, as shown in the inset in Fig. 1c. At last, we plot the m_z-image in the x-s_{arc} plane.

Results and discussion

Nanotube. Figure 1a shows the geometry structure of a nanotube. Its length is fixed at $L = 400$ nm. The outer radius and the inner radius are expressed by R and r, respectively. The thickness of the nanotube equals to R-r.

To begin, we consider the magnetization evolutions in a nanotube under the effect of magnetic field. Figure 1b shows the typical field-driven evolution of topological number Q in a nanotube, where $R = 40$ nm and $r = 20$ nm. Discontinuous changes in the Q curve indicate that the system presents different spin textures at different magnetic fields. Three different states are evolved with increasing of the magnetic field. Figure 1c–f shows the magnetic states at different H_z. At $H_z = 0$, it is a twisted helical stripe state, as the left panel in Fig. 1c shown. The corresponding m_z-image of the nanotube in x-s_{arc} plane is shown in the right panel of Fig. 1c. It shows the typical helix state, which is similar with the state in thin films[19]. For this state, its topological number $Q = 0.16$, which is close to 0. With the increasing of H_z, the topological number decreases continuously. Meanwhile, the magnetizations on the left and right sides of the nanotube rotate to the z-direction, which narrows down the helical stripes at these positions, and the magnetizations whose orientation ia along the $-z$-axis (red regions) are distributed mainly on the top and bottom of the nanotube (Fig. 1d). At $H_z = 0.25$ T, the helical stripes are completely broken on the left and right sides of the nanotube (Fig. 1e), the value of Q decreases to -7.52, and after that Q almost doesn't change with H_z. From the right panel in Fig. 1e, we can see that eight skyrmions are formed, and they are evenly distributed on the top and bottom of the nanotube. The eight skyrmions can exist until $H_z = 1.0$ T, and the size of the skyrmions decreases obviously with increasing of the H_z (Fig. 1f). The topological number Q jumps to about 4 when $H_z = 1.01$ T, which corresponds to the annihilation of four skyrmions that near the boundary, and the other four skyrmions annihilate at $H_z = 1.14$ T. The system changes to the ferromagnetic state.

It is worthy to note that in the nucleation process the topological number Q gradually increases from 0 to about 8 without any abrupt jump. This is different from the case in thin films. In thin films, the nucleation of skyrmions usually corresponds to a sudden jump of Q[39]. The skyrmions in nanotubes are created by broken of the helical stripes on the left and right sides of the nantotube, so the periodicity of the helical stripes determines the skyrmion number. According our simulation, we find the periodicity of the helical stripes is related to thickness
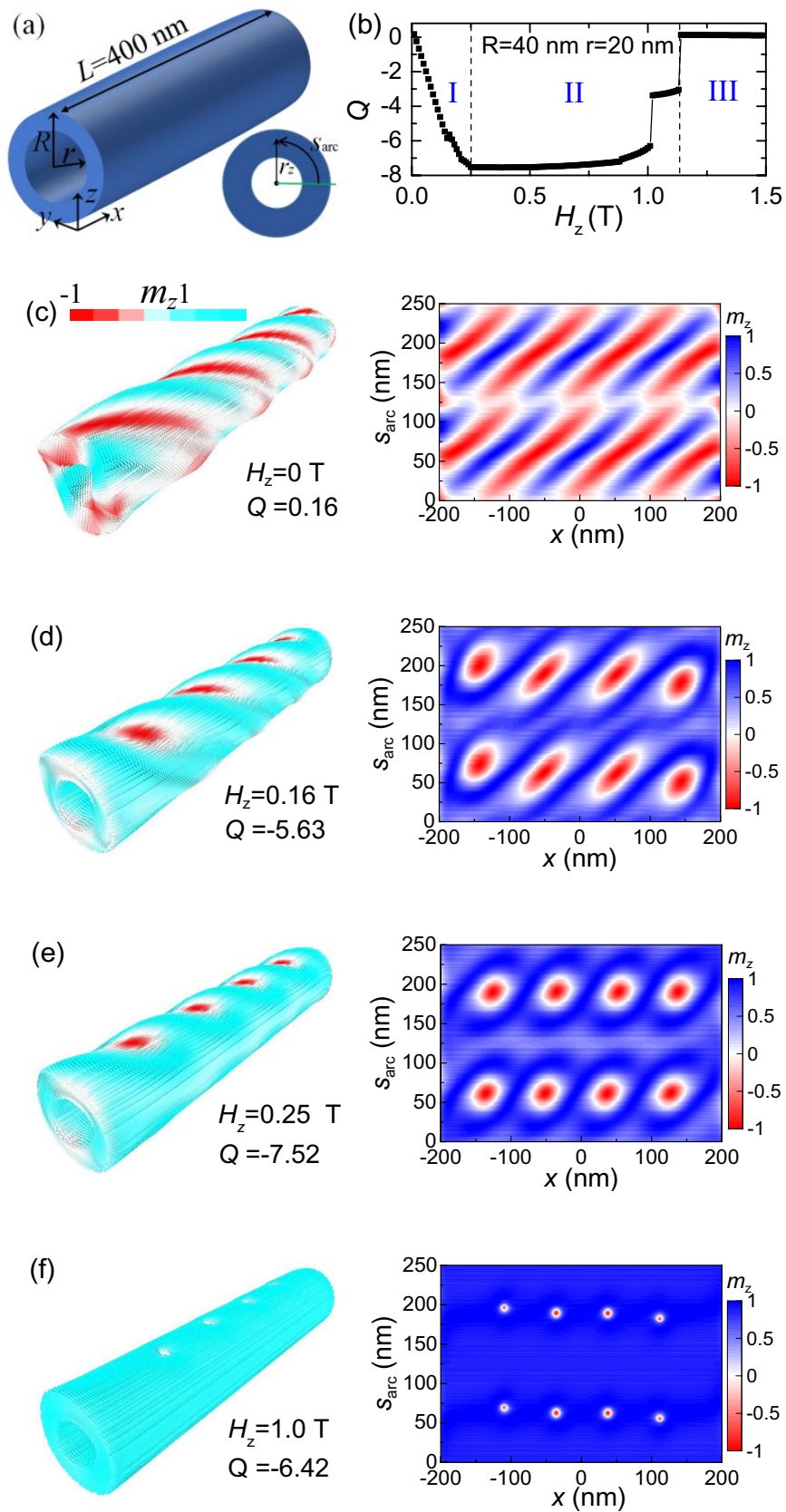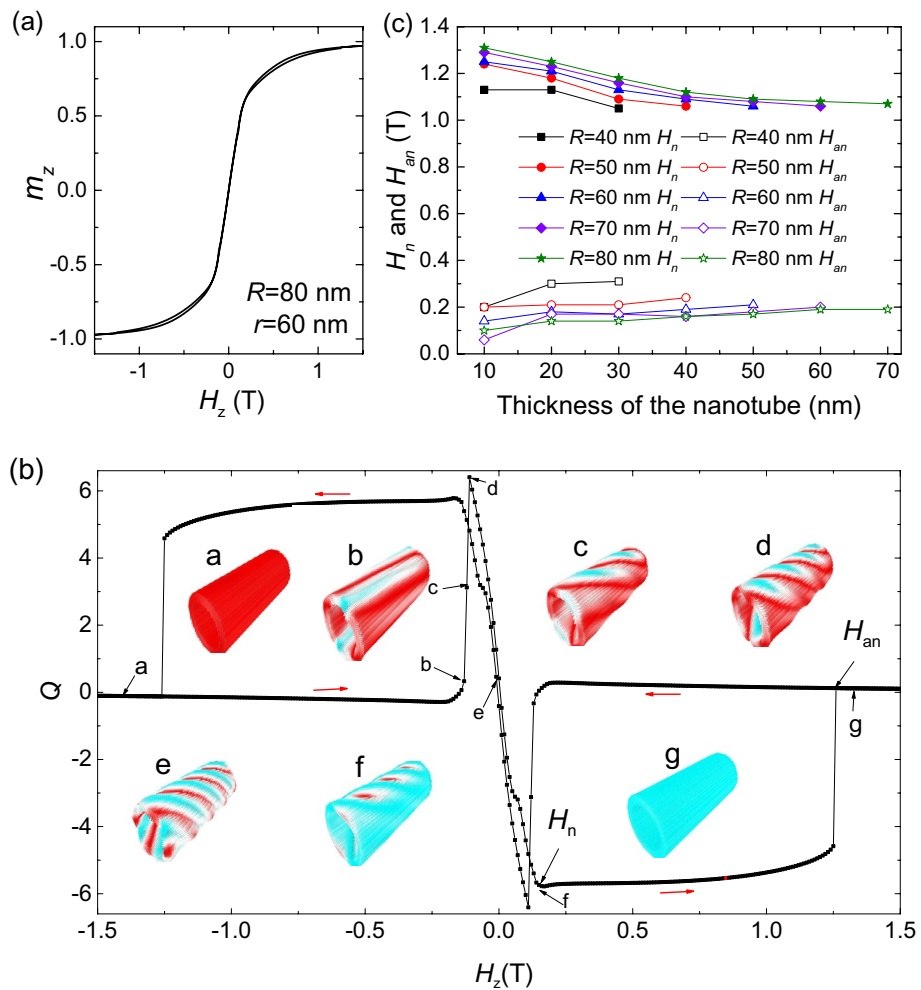
Figure 2. (**a**) The typical hysteresis loop of a nanotube ($R = 80$ nm, $r = 60$ nm) under a z-direction magnetic field. (**b**) The topological number as a function of H_z and the evolution of the magnetic structure during this process. (**c**) The size dependence of nucleation field H_n and the annihilation field H_{an} for nanotubes with different radii.

and the radius of the nanotube. For the nanotube with a smaller outer radius and a thinner thickness, it has the highest density of the helical stripes, which corresponding to more skyrmions. Instead, for the nanotube with a larger outer radius and a thicker thickness, it has the lowest density of the helical stripes and the least skyrmion number.

Then we show the hysteresis behaviors. Figure 2a shows the typical hysteresis loop of a nanotube, where $R = 80$ nm and $r = 60$ nm. The corresponding Q–curve and the typical magnetic states are shown in Fig. 2b. Starting from the uniformly magnetized system at $H_z = -1.5$ T (a). At $H_z = -0.21$ T, small stripes are formed in the nanotube. When H_z increases from -0.21 to -0.19 T, more stripes are formed, which increases the value of Q quickly to 6.2 (b–d). After that, the small stripes gradually evolve to twisted helical stripes, this evolution decreases the topological number from 6.2 to 0 (d–e). Then, the twist helical stripes become narrow on the left and right side of the nanotube. At $H_z = 0.16$ T, they are completely broken on the left and right sides of the nanotube, skyrmions are formed in the nanotube (f). We define the magnetic field that the skyrmions are formed as the nucleation field H_n. The skyrmions can stay a wide field range between $H_z = 0.15$ T and 1.25 T. At last, at $H_z = 1.26$ T, the skyrmions annihilate, the configuration of the nanotube changes to a ferromagnetic state (g). Here we define the magnetic field that the skyrmions annihilate as the annihilation field H_{an}.

Figure 2c shows the dependence of the skyrmion nucleation and annihilation field on size. The nucleation field decreases with decreasing of the nanotube thickness, however, the annihilation field increases with decreasing of the nanotube thickness. This makes the thinner nanotube has a larger field range for the existence of skyrmions. On the other hand, the nanotube has a larger radius may have a smaller nucleation field and a larger annihilation field. For example, for the nanotube ($R = 40$ nm) with thickness of 30 nm, $H_n = 0.31$ T and $H_{an} = 1.05$ T. However, for the nanotube ($R = 80$ nm) with thickness of 10 nm, H_n decreases to 0.1 T, and H_{an} increases to 1.31 T.

Now let us consider the skyrmion configuration in a nanotube. In thin films, the shape of skyrmion is circular, its magnetizations are isotropic distributed in different directions[40]. However, in a nanotube the configuration of skyrmion is different. Figure 3a shows the vector plot of the skyrmion state in a nanotube ($R = 80$ nm and
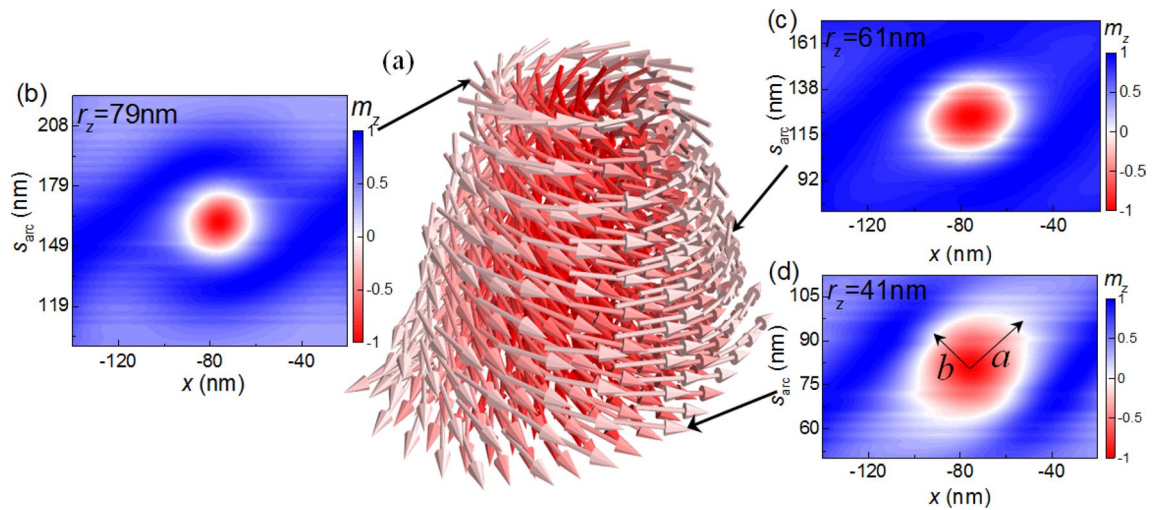
Figure 3. (**a**) Vector plot of the skymion state in a nanotube ($R = 80$ nm and $r = 40$ nm) at $H_z = 0.37$ T. (**b**)–(**d**) m_z-image in x-s_{arc} plane for different r_z.
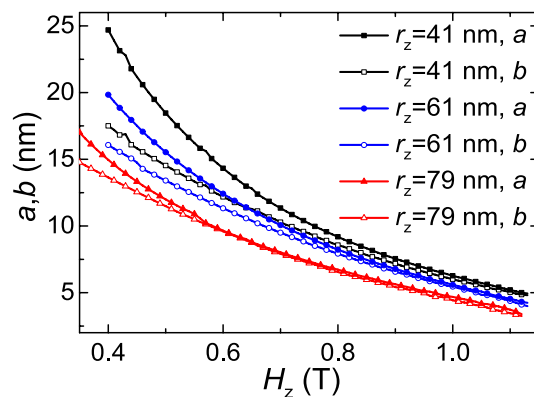
Figure 4. Variation of the skyrmion size with H_z for different r_z in the nanotube with $R = 80$ nm and $r = 40$ nm.

$r = 40$ nm) at $H_z = 0.37$ T. We can find that the shape of the skyrmion is a circular truncated cone. Figure 3b–d shows the m_z-image in x-s_{arc} plane with different r_z. It is shown that that shape of the skyrmion in each circular layer is ellipse. From the inner circular layer to the outer circular layer, the size changes a lot. In order to better describe the size of skyrmion we use ellipse to fit the boundary of the skyrmion (the isoline with $m_z = 0$). The semimajor and semiminor axis of the ellipse are represented by a and b, respectively. For $r_z = 79$ nm, *i.e.* the outer circular layer in the nanotube, $a = 14.7$ nm and $b = 13.7$ nm. When r_z decreases to 61 nm, i.e. the middle circular layer, $a = 17.4$ nm and $b = 16.1$ nm. Further, for $r_z = 41$ nm, i.e. the inner circular layer in the nanotube, $a = 24.8$ nm and $b = 19.9$ nm. These data indicate that from the outer circular layer to the inner circular layer, the skyrmion becomes larger, and the deformation becomes more obvious.

Figure 4 shows the dependence of the skyrmion size on the applied magnetic field H_z in circular films with different r_z. We can see that the difference between a and b are large in low field, but when the magnetic field increases, a and b become almost equal. Also, the size of the skyrmion is large and the deformation is obvious in the inner circular layers. For instance, for $r_z = 41$ nm, at $H_x = 0.4$ T, $a = 24.8$ nm, $b = 19.9$ nm, and the value of $a - b = 4.9$ nm. However, for $r_z = 79$ nm, a, b and $a - b$ decrease to 7.5 nm, 7.3 nm and 0.2 nm at $H_x = 0.9$ T.

Curved thin film. We also study the magnetization evolution in curved magnetic films. The model is shown in Fig. 5a. We first choose a thin film (the left panel). Its length $L = 400$ nm, width $W = 250$ nm, and thickness $H = 10$ nm. Then, we curve the thin film to a circularly curved film with a fixed radius R, where R varies from 40 nm to infinity. We calculate the hysteresis behaviors under a magnetic field along z-axis for these circularly curved films.

Figure 5b shows the typical hysteresis loops for the curved films with R. We find that with decreasing of R, the remanence increases and the coercivity decreases. The susceptibility at $H_z = 0$ ($\chi(0)$) increases with decreasing of R. Figure 5c shows the value of $\chi(0)$ as a function of R. We can find that when R > 150 nm, $\chi(0)$ slightly increases with decreasing of R. However, when R < 150 nm, $\chi(0)$ rapidly increases with decreasing of R. Particularly, as R
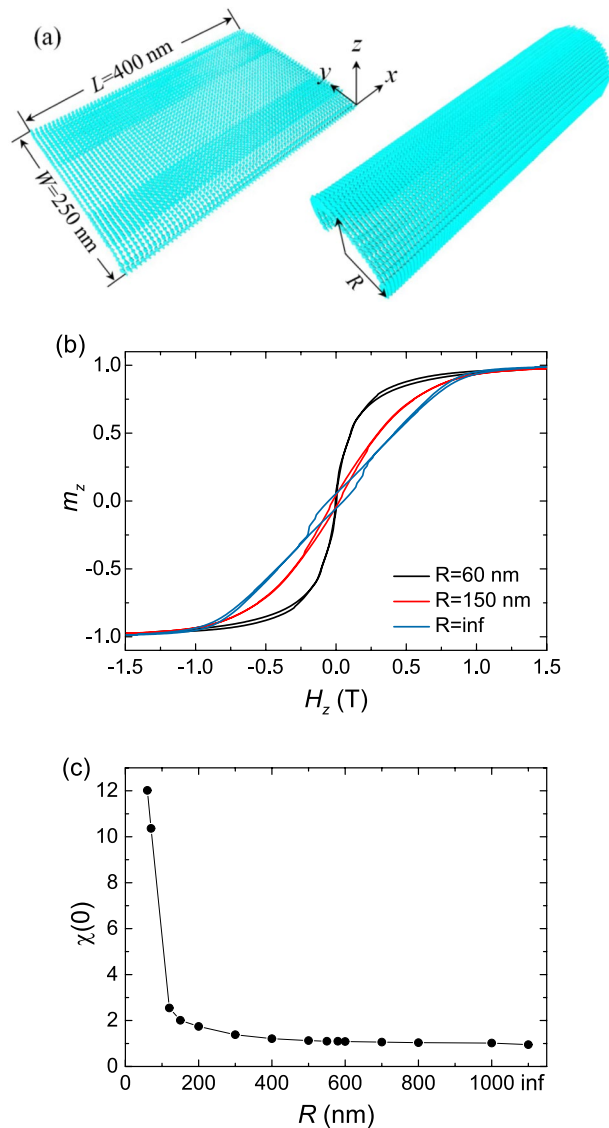
Figure 5. (**a**) The sketch of the curved film. The size of the film is fixed at length of 400 nm, width of 250 nm, and thickness of 10 nm. Then, it is curved to a circularly curved film with a fixed radius R, where R varies from 40 nm to infinity. (**b**) The hysteresis loops for the curved films with $R = 60$, 150 and inf, respectively. (**c**) The susceptibility at $H_z = 0$ as a function of R.

decreases to 70 nm, $\chi(0)$ increased to 10.4. For the case of the two-dimensional thin film ($R = $inf), the hysteresis loop that we calculated is similar to the measurement results in Ref.[41].

Next, we will show the evolution of magnetic states during these hysteresis processes. There are three different types of evolution process. Figures 6, 7 and 8 show the typical Q-curves for these three types, and the represented magnetic states are shown as insets.

For $R > 600$ nm, the evolution of magnetic states is similar to the case of thin film ($R = $ inf). A typical field-driven evolution of the magnetic state is shown in Fig. 6, where $R = $ inf, i.e. the rectangular thin film. When magnetic field increases from -1.5 to 0.11 T, the magnetic state gradually changes from the uniformly magnetized state to the maze domains (a–e). The topological number changes slightly, it almost equals to 0. Then when the magnetic field gradually increases from 0.11 to 0.61 T, the topological number shows some small jumps and slowly decreases, the maze domain gradually shrinks to a distorted nanostripe (f–i). At $H_z = 0.62$ T, the topological number shows a sudden jump, meanwhile the distorted nanostripe breaks, three skyrmions are formed in the thin film (i, j). The skyrmions can exist in a wide field range between $H_z = 0.62$ T and 1.41 T. At last, at $H_z = 1.42$ T, the skyrmions annihilate, the configuration of the thin film changes to the ferromagnetic state (k).

For 150 nm $\leq R < 600$ nm, the typical field-driven evolution of the magnetic state is shown in Fig. 7, where $R = 150$ nm. The Q-curve is different from the case in Fig. 6. In this region, there is no formation of skymion during the hysteresis process. Starting from the saturated ferromagnetic state (a), a stripe domain (b) is gradually formed in the curved film with the magnetic field increasing from -1.5 to -0.29 T. The topological number almost doesn't change in this process. When the magnetic field is greater than -0.29 T, the topological number
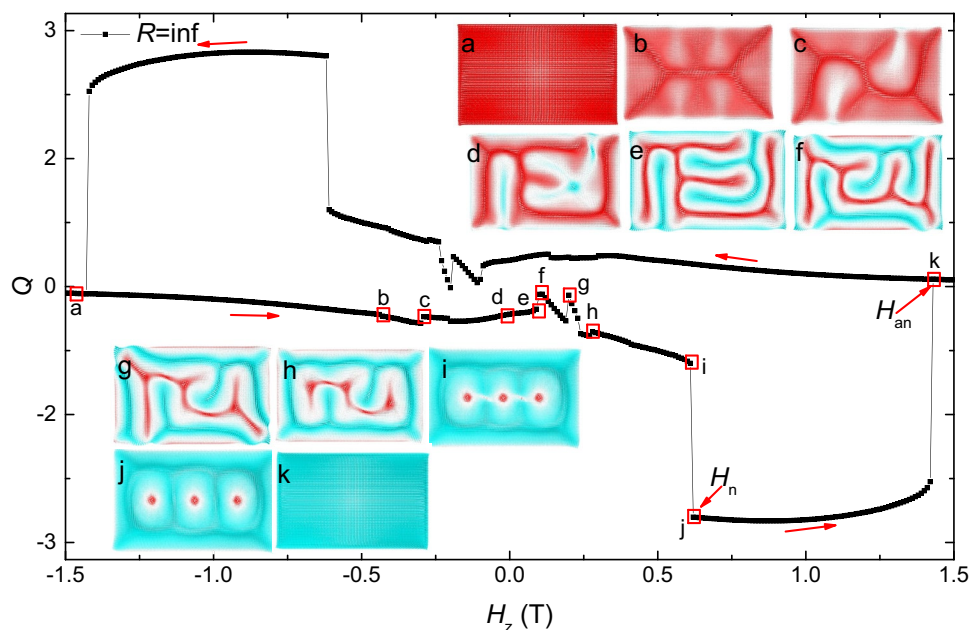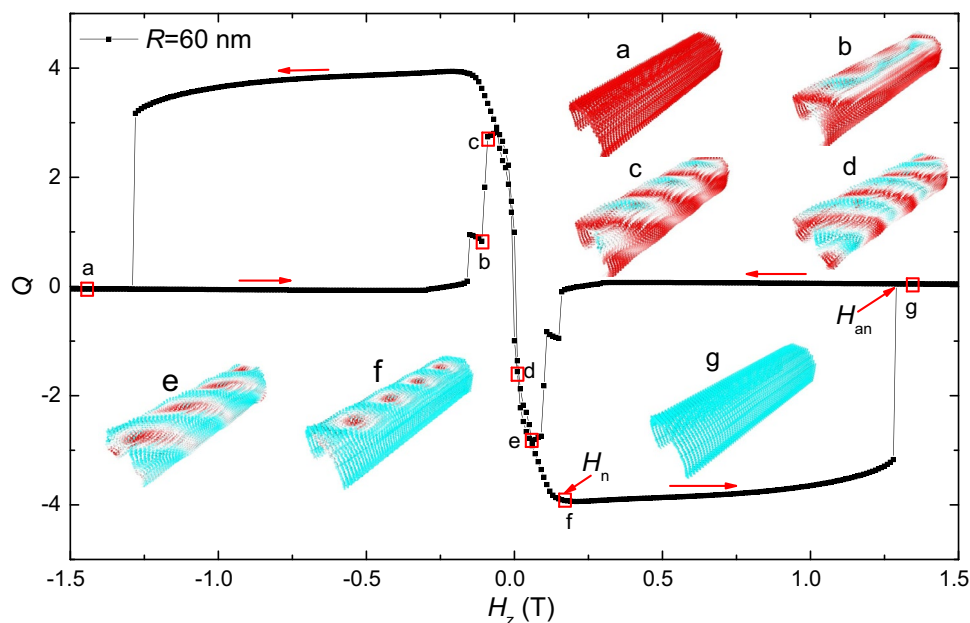
Figure 6. The topological number as a function of H_z and the evolution of the magnetic structure during this hysteresis process in the thin film ($R = \inf$).
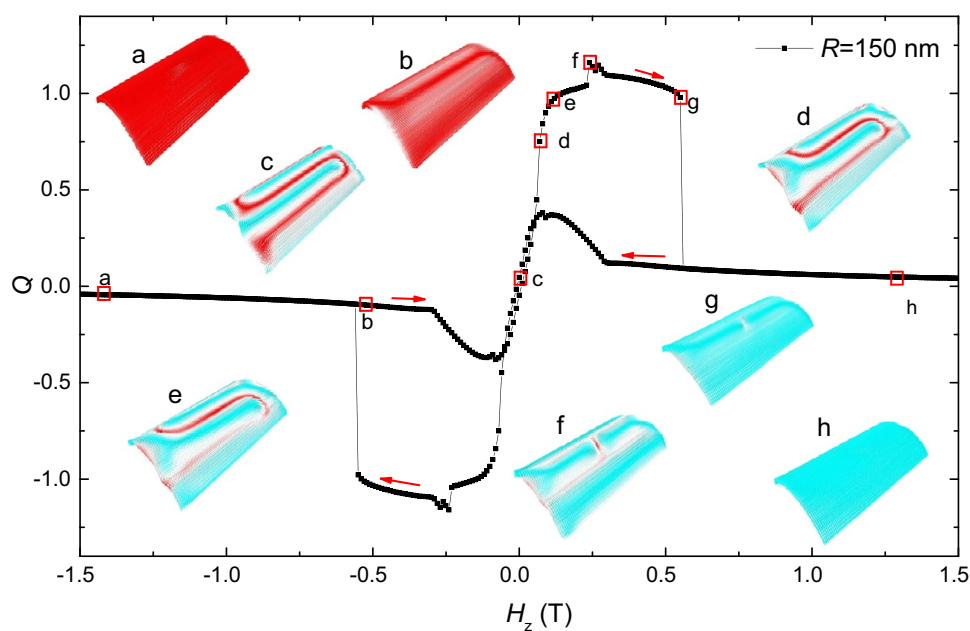

Figure 7. The topological number as a function of H_z and the evolution of the magnetic structure during this process in the circular curved film with $R = 150$ nm.

decreases first and then increases to about 1 (c–f). Although the topological number is about 1, it doesn't indicate that a skyrmion is formed, it is just originated from the two ends of the nanostripe. At $H_z = 0.56$ T, the sudden drop of Q from 1 to 0 indicates the disappearance of nanostripe and formation of the ferromagnetic state (g, h).

For $R < 150$ nm, the typical field-driven evolution of the magnetic state is shown in Fig. 8, where $R = 60$ nm. This dynamical process is similar to the case in nanotubes. At $H_z = -1.5$ T, all magnetizations in the curved film uniformly point to the z-axis (a), and the topological number is zero. The ferromagnetic state stays until H_z increases to -0.16 T. Then, stripes appear in the system, and the stripes gradually twist (b–d). In this process, the value of Q shows a great change. It first increases to about 2.8 at $H_z = -0.09$ T, and then decreases to -3.93 at $H_z = 0.17$ T. We can find four skyrmions are formed in the curved film at $H_z = 0.17$ T, which is formed by broken of the helical stripes on the left and right sides of the curved film. This dynamical process is similar to the case in

Figure 8. The topological number as a function of H_z and the evolution of the magnetic structure during this process in the circular curved film with $R = 60$ nm.
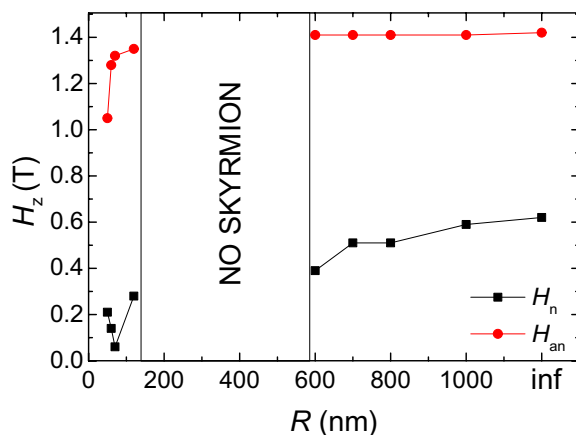
Figure 9. The nucleation field and annihilation field in curved films as a function of R.

nanotubes. These skyrmions can stay in a wide field range between $H_z = 0.17$ T and 1.29 T. At last, at $H_z = 1.3$ T, the skyrmions annihilate, the configuration of the curved film changes to the ferromagnetic state.

From the above description, we can find that the skyrmions are evolved from stripes. The curved radius has a big influence on this transition state. For large radius, the curvature has a little influence on the system energy, it shows maze domains. However, when the radius is less than 600 nm, the shape anisotropy induced by the curvature stretches the stripe to straight, and the stripes that parallel to the x-axis are preferred. These straight stripes cannot evolve to skyrmions. For small radius, the effect of the curvature becomes more obvious, the stripes twist along the surface of the curved film, the twisted stripes break to skyrmions. Thus, we can say the curvature influences the shape of the stripes that formed in the curved film, so three different kinds of evolutionary processes are found.

The curvature also influences the nucleation and annihilation fields of skyrmions. Figure 9 shows the radius dependence of the nucleation and annihilation fields of skyrmions in the circular curved magnetic film. For $R > 600$ nm, the nucleation field H_n slightly increases with R, however, the annihilation field H_{an} doesn't change. For $R < 150$ nm, the nucleation field H_n is smaller than the case of $R > 600$ nm. It has the smallest value (0.1 T) when $R = 70$ nm.

We know that the challenge for using magnetic skyrmions in applications is to find room temperature-stabled skyrmions without external force. Recently, several experiments have demonstrated that ultrathin ferromagnetic/heavy metal multilayers are good structures that can host skyrmions at zero magnetic field and room temperature[42–44], and its size and density also can be controlled by the shape and size of the nanostructure[44]. Our
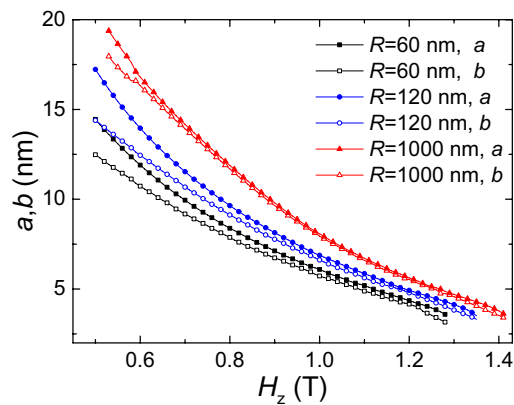
Figure 10. The size of skyrmion as a function of the magnetic field H_z in curved films with different R.

above results show an evidence that curvature is also a method to reduce the magnetic field to stabilize skyrmions. Thus, we can predict that if we use the suitable parameters, we may observe room temperature-stabled skyrmions at zero magnetic field, and we can control its stability by curvature. This is the next aim of our future study.

The size of the skyrmion in the curved films also depends on R. Figure 10 shows the dependence of the skyrmion size on the applied magnetic field H_z for different R. We also use a and b to denote the semimajor and semiminor axis of the ellipse. In curved film with larger R ($R = 1000$ nm), the value of a and b is almost equal. With decreasing of R, the difference between a and b becomes larger. Overall, the size of the skyrmion in curved film with smaller R is smaller than the ones in curved film with larger R.

Conclusion

In summary, in this work we studied the magnetization evolution in three-dimensional chiral nanostructure, including nanotubes and circularly curved thin films. We found that the nucleation of skyrmion in nanotube is realized by broken of the helical stripes on the left and right sides of the nanotube without abrupt change of topological number. The nucleation field decreases, but the annihilation field increases with decreasing of the nanotube thickness. The shape of the skyrmion is a circular truncated cone. From the outer circular layer to the inner circular layer, the skyrmion becomes larger, and the deformation becomes more obvious. In curved magnetic films with fixed arc. There are three different kinds of hysteresis processes are found. For R > 600 nm, the behaviors are similar with the case of 2D thin film. For 150 nm $\leq$ R < 600 nm, no skyrmion is formed in the hysteresis process. For R < 150 nm, the skyrmions are created by broken of the helical stripes on the left and right sides of the curved film.

References
 1. Streubel, R. *et al.* Magnetism in curved geometries. *J. Phys. D Appl. Phys.* **49**, 363001 (2016).
 2. Ferna'ndez-Pacheco, A. *et al.* Three-dimensional nanomagnetism. *Nat. Commun.* **8**, 15756 (2017).
 3. Sheka, D. D. *et al.* Curvature effects in statics and dynamics of low dimensional magnets. *J. Phys. A Math. Theor.* **48**, 125202 (2015).
 4. Gaididei, Y., Kravchuk, V. P. & Sheka, D. D. Curvature effects in thin magnetic shells. *Phys. Rev. Lett.* **112**, 257203 (2014).
 5. Hertel, R. Curvature-induced magnetochirality. *SPIN* **3**, 1340009 (2013).
 6. Da Col, S. *et al.* Observation of Bloch-point domain walls i39n cylindrical magnetic nanowires. *Phys. Rev. B* **89**, 180405 (2014).
 7. Biziere, N. *et al.* Imaging the fine structure of a magnetic domain wall in a Ni nanocylinder. *Nano Lett.* **13**, 2053–2057 (2013).
 8. Pylypovskyi, O. V. *et al.* Coupling of chiralities in spin and physical spaces: the Möbius ring as a case study. *Phys. Rev. Lett.* **114**, 197204 (2015).
 9. Kravchuk, V. P. *et al.* Out-of-surface vortices in spherical shells. *Phys. Rev. B* **85**, 144433 (2012).
10. Otálora, J. A., López-López, J. A., Vargas, P. & Landeros, P. Chirality switching and propagation control of a vortex domain wall in ferromagnetic nanotubes. *Appl. Phys. Lett.* **100**, 072407 (2012).
11. Smith, E. J. *et al.* Magnetic microhelix coil structures. *Phys. Rev. Lett.* **107**, 097204 (2011).
12. Yan, M., Kákay, A., Andreas, C. & Hertel, R. Spin-Cherenkov effect and magnonic Mach cones. *Phys. Rev. B* **88**, 220412(R) (2013).
13. Mühlbauer, S. *et al.* Skyrmion lattice in a chiral magnet. *Science* **323**, 915–919 (2009).
14. Fert, A., Cros, V. & Sampaio, J. Skyrmions on the track. *Nat. Nanotechnol.* **8**, 152–156 (2013).
15. Wiesendanger, R. Nanoscale magnetic skyrmions in metallic films and multilayers: a new twist for spintronics. *Nat. Rev. Mater.* **1**, 16044 (2016).
16. Zhang, X., Ezawa, M. & Zhou, Y. Magnetic skyrmion logic gates: conversion, duplication and merging of skyrmions. *Sci. Rep.* **5**, 9400 (2015).
17. Kiselev, N. S., Bogdanov, A. N., Schäfer, R. & Rößler, U. K. Chiral skyrmions in thin magnetic films: new objects for magnetic storage technologies?. *J. Phys. D Appl. Phys.* **44**, 392001 (2011).
18. Zhou, Y. Magnetic skyrmions: intriguing physics and new spintronic device concepts. *Natl. Sci. Rev.* **6**, 210–212 (2019).
19. Yu, X. Z. *et al.* Near room-temperature formation of a skyrmion crystal in thin-films of the helimagnet FeGe. *Nat. Mater.* **10**, 106–109 (2011).
20. Yu, X. Z. *et al.* Real-space observation of a two-dimensional skyrmion crystal. *Nature* **465**, 901–904 (2010).
21. Seki, S., Yu, X. Z., Ishiwata, S. & Tokura, Y. Observation of skyrmions in a multiferroic material. *Science* **336**, 198–201 (2012).

22. Kézsmárki, I. *et al.* Néel-type skyrmion lattice with confined orientation in the polar magnetic semiconductor GaV$_4$S$_8$. *Nat. Mater.* **14**, 1116–1122 (2015).
23. Yadav, A. K. *et al.* Observation of polar vortices in oxide superlattices. *Nature* **530**, 198–201 (2016).
24. Jiang, W. *et al.* Blowing magnetic skyrmion bubbles. *Science* **349**, 283–286 (2015).
25. Woo, S. *et al.* Observation of room-temperature magnetic skyrmions and their current-driven dynamics in ultrathin metallic ferromagnets. *Nat. Mater.* **15**, 501–506 (2016).
26. Tolley, R., Montoya, S. A. & Fullerton, E. E. Room-temperature observation and current control of skyrmions in Pt/Co/Os/Pt thin film. *Phys. Rev. Mater.* **2**, 044404 (2018).
27. Jia, M., Yan, H. & Liu, Y. Effect of anisotropy on the evolution of magnetic configuration in a helimagnet nanodisk. *J. Magn. Magn. Mater.* **426**, 155–158 (2017).
28. Johnson, P., Gangopadhyay, A. K., Kalyanaraman, R. & Nussinov, Z. Demagnetization-borne microscale skyrmions. *Phys. Rev. B* **86**, 064427 (2012).
29. Kravchuk, V. P. *et al.* Topologically stable magnetization states on a spherical shell: curvature-stabilized skyrmions. *Phys. Rev. B* **94**, 144402 (2016).
30. Kravchuk, V. P. *et al.* Multiplet of skyrmion states on a curvilinear defect: reconfigurable skyrmion lattices. *Phys. Rev. Lett.* **120**, 067201 (2018).
31. Wang, X. *et al.* Current-induced skyrmion motion on magnetic nanotubes. *J. Phys. D Appl. Phys.* **52**, 225001 (2019).
32. Huo, X. & Liu, Y. The stability of a skyrmion in a nanotube. *New J. Phys.* **21**, 093924 (2019).
33. Rüffer, D. *et al.* Magnetic states of an individual Ni nanotube probed by anisotropic magnetoresistance. *Nanoscale* **4**, 4989–4995 (2012).
34. Albrecht, T. R. *et al.* Bit patterned media at 1 Tdot/in^2 and beyond. *IEEE Trans. Magn.* **49**, 773–778 (2013).
35. Bachmann, J. *et al.* Ordered Iron oxide nanotube arrays of controlled geometry and tunable magnetism by atomic layer deposition. *J. AM. Chem. Soc.* **129**, 9554–9555 (2007).
36. Vansteenkiste, A. *et al.* The design and verification of MuMax3. *AIP Adv.* **4**, 107133 (2014).
37. Beg, M. *et al.* Ground state search, hysteretic behaviour, and reversal mechanism of skyrmionic textures in confined helimagnetic nanostructures. *Sci. Rep.* **5**, 17137 (2015).
38. Nagaosa, N. & Tokura, Y. Topological properties and dynamics of magnetic skyrmions. *Nat. Nanotechnol.* **8**, 900 (2013).
39. Du, H., Ning, W., Tian, M. & Zhang, Y. Field-driven evolution of chiral spin textures in a thin helimagnet nanodisk. *Phys. Rev. B* **87**, 014401 (2013).
40. Romming, N. *et al.* Field-dependent size and shape of single magnetic skyrmions. *Phys. Rev. Lett.* **114**, 177203 (2015).
41. Huang, S. X. & Chien, C. L. Extended skyrmion phase in epitaxial FeGe(111) thin films. *Phys. Rev. Lett.* **108**, 267201 (2012).
42. Boulle, O. *et al.* Room-temperature chiral magnetic skyrmions in ultrathin magnetic nanostructures. *Nat. Nanotechnol.* **11**, 449–454 (2017).
43. Brandão, J., Dugato, D. A., Puydinger dos Santos, M. V. & Cezar, J. C. Evolution of zero-field ferrimagnetic domains and skyrmions in exchange-coupled Pt/CoGd/Pt confined nanostructures: implications for antiferromagnetic devices. *ACS Appl. NanoMater.* **2**, 7532–7539 (2019).
44. Brandão, J. *et al.* Observation of magnetic skyrmions in unpatterned symmetricmultilayers at room temperature and zero magnetic field. *Sci. Rep.* **9**, 4144 (2019).

Acknowledgements

Author contributions

N.C. and X.Y. plotted the figures, S.X. calculated the data, Y. L. wrote the paper.

Competing interests

The authors declare no competing interests.

Additional information

Correspondence and requests for materials should be addressed to Y.L.

Reprints and permissions information is available at www.nature.com/reprints.

Publisher's note Springer Nature remains neutral with regard to jurisdictional claims in published maps and institutional affiliations.